THE USE OF DFT IN CATALYST DEVELOPMENT

Harry Winston Sullivan
Chemical Engineering
University of Utah
Salt Lake City
h.sully2015@gmail.com

ABSTRACT

Gaining a mechanistic understanding of the role that catalysts play in chemical processes is essential for enhancing their efficiency, rate, and recyclability. Yet, there exists a notable challenge in completely characterizing a reaction using experimental data alone. This challenge has spurred the development of computational methods designed not only to replicate existing experimental results but also to provide deeper insights that go beyond what can be achieved through purely experimental means. Electronic structure theory and specifically density functional theory (DFT) aim to achieve this through the characterization of potential energy surfaces. With access to the surface, a computational chemist can run optimization procedures to discover energy minima and saddle points. These points are paramount as they characterize the path chemical reactions take. This paper aims to review the basic theory, catalytic applications, and an example calculation to give new chemists and chemical engineers a resource to break into electronic structure theory.

Keywords Density Functional Theory · Catalysis · Reaction Pathway Discovery · Electronic Properties of Catalytic Materials

1 Introduction

As we strive for more sustainable and efficient chemical reactors, understanding the underlying mechanisms of the catalysts they use becomes primary. In this pursuit, conventional methods of characterization are commonplace. Through the utilization of methods such as Fourier transform infrared spectroscopy (FTIR) [1], X-ray scattering [2], and various electron microscopes [3] researchers can peer into the atomic scale of catalytic materials. While these are valuable, they do little to shed light on the reaction mechanisms themselves. In order to effectively understand a catalyst, access to the angstrom-scale dynamics as a reaction proceeds is necessary. With the advent of powerful graphics processing units [4] and cluster super computers, computational quantum chemistry methods have emerged as invaluable tools for unraveling complex reaction pathways at the atomic and molecular levels [5].

The most prolific of these tools is density functional theory (DFT). DFT is rooted in the principles of electronic structure and has gained prominence in catalysis as a powerful technique for characterizing catalytic processes [6]. The aim of this paper is to inform new researchers on all the tools required to make novel research contributions in catalysis using DFT. Why might a researcher hope to learn DFT? Given enough computational resources, DFT can model almost any observable while having top tier accuracy. As an example, FTIR contains vital information on the vibrational modes of a material. By analyzing the outputted energy surfaces, researchers have shown a clear link between energy wells and FTIR frequency modes [7]. X-ray scattering and electron microscopes can show the equilibrium geometries of a catalyst [8], however the same information can be found by analyzing stable points in a DFT energy surface. To list a few more achievable outputs from a DFT calculation, DFT can: obtain excited states found in UV/VIS spectra, reproduce NMR spectra, CD spectra [9], and polarizability [10]. DFT can discover reaction barrier heights, suggest reaction pathways [10], obtain reaction rates, and reproduce thermodynamic properties [11][12].

The forthcoming structure will be as follows, first we will explore the basics of electron structure theory and the Born-Oppenheimer approximation. This will then be followed by an explanation of the Hohenberg-Kohn theorems that are fundamental to DFT. With these out of the way, we can then embark on the specific details of running DFT

calculations using the Kohn-Sham method. With the method established, reaction pathway discovery can then be elucidated. Finally, the narrative culminates with a discussion of practical applications in catalysis, where the theoretical insights are translated into real-world contexts, showcasing the power of DFT for understanding catalytic systems.

2 Theory

2.1 Electronic Structure Theory and the Born-Oppenheimer Approximation

The fundamental equation that electron structure theory aims to solve is the non-relativistic time independent Schrodinger equation. This equation is an Eigenfunction Eigenvalue relation. It is meant to relate the wave function of a many-body system of nuclei and electrons to its corresponding energy.

$$\hat{\mathbf{H}}\psi = E\psi \tag{1}$$

$$\psi = \psi(x_1, y_1, z_1, \omega_1, ..., x_N, y_N, z_N, \omega_N) \tag{2}$$

Each argument in the wave function corresponds to each particles x, y, z position and their spin ω. With the form of the wave function established we can consider what the Hamiltonian is in atomic units:

$$\hat{\mathbf{H}} = -\sum_{A}^{\text{Nucl.}} \frac{1}{2M_A}\nabla_A^2 - \sum_{i}^{\text{Elec.}} \frac{1}{2}\nabla_i^2 - \sum_{A}^{\text{Nucl.}}\sum_{i}^{\text{Elec.}} \frac{Z_A}{r_{i,A}} + \sum_{i}^{\text{Elec.}}\sum_{j>i}^{\text{Elec.}} \frac{1}{r_{i,j}} + \sum_{A}^{\text{Nucl.}}\sum_{B>A}^{\text{Nucl.}} \frac{Z_A Z_B}{r_{A,B}} \tag{3}$$

Each term corresponds to the kinetic energy of the nuclei, the kinetic energy of the electrons, the electron-nuclei attraction, the electron-electron repulsion, and the nuclei-nuclei repulsion respectively. This equation can be further simplified by claiming that the nuclei move so much slower than the electrons, they might as well be frozen. This assumption is not that unrealistic. Even with only one proton, the nucleus is almost 2 million times heavier than and electron and correspondingly their characteristic timescales. This is called the Born-Oppenheimer (BO) approximation [13]. This gives an electronic Hamiltonian as well as a "clamped" nucleus Schrodinger equation. We also can reduce notation by considering electron co-ordinates as $\mathbf{r}$ and nucleus co-ordinates as $\mathbf{R}$[1].

$$\hat{\mathbf{H}}_{\text{Elec.}}(\mathbf{r};\mathbf{R}) = -\sum_{i}^{\text{Elec.}} \frac{1}{2}\nabla_i^2 - \sum_{A}^{\text{Nucl.}}\sum_{i}^{\text{Elec.}} \frac{Z_A}{r_{i,A}} + \sum_{i}^{\text{Elec.}}\sum_{j>i}^{\text{Elec.}} \frac{1}{r_{i,j}} + \sum_{A}^{\text{Nucl.}}\sum_{B>A}^{\text{Nucl.}} \frac{Z_A Z_B}{r_{A,B}} \tag{4}$$

$$\hat{\mathbf{H}}_{\text{Elec.}}(\mathbf{r};\mathbf{R})\psi_{\text{Elec.}}(\mathbf{r};\mathbf{R}) = E_{\text{Elec.}}(\mathbf{R})\psi_{\text{Elec.}}(\mathbf{r};\mathbf{R}) \tag{5}$$

It is traditional to include the nuclear repulsion in this Hamiltonian, it allows later calculations to be done more easily. We can also note that the inclusion of this term makes no overall difference to the motion of the electrons. The nuclei are immobile, therefore they just contribute a constant to the Hamiltonian. This simply shifts the Eigenvalues up/down, while making no change to the Eigenfunctions. We can write the original ψ in terms of a summation of $\psi_{\text{Elec.}}$:

$$\psi(\mathbf{r},\mathbf{R}) = \sum_{k} \psi_{\text{Elec.},k}(\mathbf{r};\mathbf{R})\chi_k(\mathbf{R}) \tag{6}$$

It can then by shown by inserting ψ into the Schrodinger equation that we attain the following relation for $\chi_k(\mathbf{R})$[2]:

$$\left(-\sum_{A}^{\text{Nucl.}} \frac{1}{2M_A}\nabla_A^2 - \sum_{A}^{\text{Nucl.}} \frac{1}{2M_A} \langle \psi_k(\mathbf{r};\mathbf{R}) | \nabla_A^2 | \psi_k(\mathbf{r};\mathbf{R}) \rangle + E_{\text{Elec.}}(\mathbf{R}) \right) \chi_k(\mathbf{R}) = E\chi_k(\mathbf{R}) \tag{7}$$

We can then define two different terms:

[1] This means writing $\mathbf{r}$ is the same as writing $x_1, y_1, z_1, \omega_1, ..., x_N, y_N, z_N, \omega_N$ where every x, y, z is an electron. Similarly for the nuclei.

[2] This can be considered a nuclei wave-function

$$(\hat{\mathbf{T}}_N(\mathbf{R}) + \hat{\mathbf{U}}_N(\mathbf{R}))\chi_k(\mathbf{R}) = E\chi_k(\mathbf{R}) \tag{8}$$

$$\hat{\mathbf{T}}_N(\mathbf{R}) = -\sum_A^{\text{Nucl.}} \frac{1}{2M_A}\nabla_A^2 \tag{9}$$

$$\hat{\mathbf{U}}_N(\mathbf{R}) = -\sum_A^{\text{Nucl.}} \frac{1}{2M_A}\langle\psi_k(\mathbf{r};\mathbf{R})|\nabla_A^2|\psi_k(\mathbf{r};\mathbf{R})\rangle + E_{\text{Elec.}}(\mathbf{R}) \tag{10}$$

This is the nuclear Schrodinger equation. This type of setup is essentially treating $E_{\text{Elec.}}$ as a potential energy surface for the nuclei to move around on. The extra gradient term in the potential energy is often neglected as it is usually inconsequential to the overall calculation. A quantification of its significance can be found in reference [14]. This establishes the fundamental problem electronic structure theory aims to solve. For ease of reference the electronic sub problem is repeated.

$$\hat{\mathbf{H}}_{\text{Elec.}}(\mathbf{r};\mathbf{R})\psi_{\text{Elec.}}(\mathbf{r};\mathbf{R}) = E_{\text{Elec.}}(\mathbf{R})\psi_{\text{Elec.}}(\mathbf{r};\mathbf{R}) \tag{11}$$

To solve the electronic Schrodinger equation, scientists have developed numerous methods. To name a few: Hartree Fock basis set methods [15], semi-empirical Hartree Fock approximations [16], couple cluster theory [17], many body perturbation theory [17], and the main focus of this paper density functional theory[18].

2.2 Kohn Sham Density Functional Theory

Density functional theory starts with two theorems proposed by Hoenberg and Kohn in 1964 [18]. They showed that the ground state properties of a many body electron system depend only on the electron density $\rho(x, y, z)$. By treating the electrons as a density rather than a collection of particles we can solve the problem in a similar manner to classical fluid mechanics approach. Effectively, this reduces the problem of finding a wave function with $3N$ electron positions $\mathbf{r}$ as arguments to finding a function with only 3 in certain cases. Their ground breaking work also showed that the correct ground state energy is the one that minimizes the energy functional of the electron density $E_{\text{Elec.}}[\rho(x, y, z)]$. This hints at a method of discovering the ground state energy, and therefore the potential energy surface that nuclei move upon. DFT has improved upon the established Hartree Fock theory through the inclusion of electron exchange and correlation effects, as well as allowing the possibility for algorithmic speed ups.

Supposing we knew the function $\rho(x, y, z)$, we can then compute it's energy through the energy functional. By then taking a variational derivative with respect to the density, we can then update our beliefs and iterate until we find the optimal density. The weakness of the DFT method is that we don't know the exact energy functional. Through our knowledge of the electronic Hamiltonian, we can make guesses as to its form. It will contain an electron kinetic energy (although the exact form of this functional is not clear), a Coulomb repulsion term, and a Coulomb attraction term to the nuclei. These terms do not directly contain the repulsive effects due to the Pauli exclusion principle [19], nor does it contain the anti symmetry (exchange effects) of the electron wave function. Additionally, there is correlation effects that we must consider.

An initial attempt to resolve the lack of a clear optimization method was found by Kohn and Sham in 1965 [20]. Taking inspiration from Hartree Fock theory [15], they assume that the wave function can be written in terms of a Slater determinant [21]. To define the density, then consequentially the kinetic energy we first must understand the basic ideas behind Hartree Fock. In order to simplify the problem, Hartree proposed writing the electronic wave function as a product of "orbitals" ϕ [15].[3]

$$\psi_{\text{HP}}(\mathbf{r}_1, \mathbf{r}_2, ...\mathbf{r}_i) = \phi_1(\mathbf{r}_1)\phi_2(\mathbf{r}_2)...\phi_N(\mathbf{r}_N) \tag{12}$$

Immediately, one can see that the Hartree product approach does not work. Electrons are supposed to be mathematically indistinguishable particles. Due to electrons being Fermions, when we exchange two different electron arguments we should expect the wave function to stay the same apart from a sign change. To convince you this, consider a two particle case:

[3]Noting that the implicit parametric dependence on the nuclei positions is omitted

$$\psi_{\text{HP}}(\mathbf{r}_1, \mathbf{r}_2) = \phi_1(\mathbf{r}_1)\phi_2(\mathbf{r}_2) \tag{13}$$

Then exchanging the arguments gives:

$$\psi_{\text{HP}}(\mathbf{r}_2, \mathbf{r}_1) = \phi_1(\mathbf{r}_2)\phi_2(\mathbf{r}_1) \tag{14}$$

This does not change signs, and the overall wave function changes as ϕ_1 is not necessarily the same as ϕ_2. To resolve this, one can force ψ to have anti-symmetry do this by construction.

$$\psi(\mathbf{r}_1, \mathbf{r}_2) = \frac{1}{\sqrt{2}} \begin{vmatrix} \phi_1(\mathbf{r}_1) & \phi_2(\mathbf{r}_1) \\ \phi_1(\mathbf{r}_2) & \phi_2(\mathbf{r}_2) \end{vmatrix} = \frac{1}{\sqrt{2}} \Big(\phi_1(\mathbf{r}_1)\phi_2(\mathbf{r}_2) - \phi_1(\mathbf{r}_2)\phi_1(\mathbf{r}_2) \Big) = -\psi(\mathbf{r}_2, \mathbf{r}_1) \tag{15}$$

For an N electron system the Slater determinant [21] looks like:

$$\psi(\mathbf{r}_1, \mathbf{r}_2, ...\mathbf{r}_N) = \frac{1}{\sqrt{N}} \begin{vmatrix} \phi_1(\mathbf{r}_1) & \phi_2(\mathbf{r}_1) & \cdots & \phi_N(\mathbf{r}_1) \\ \phi_1(\mathbf{r}_2) & \phi_2(\mathbf{r}_2) & \cdots & \phi_N(\mathbf{r}_2) \\ \vdots & \vdots & \ddots & \vdots \\ \phi_1(\mathbf{r}_N) & \phi_2(\mathbf{r}_N) & \cdots & \phi_N(\mathbf{r}_N) \end{vmatrix} \sim |ij \cdots k\rangle \tag{16}$$

Where $|ij \cdots k\rangle$ is a commonly used shorthand. With our wave function, we can write down the spacial electron density [20].

$$\rho(x, y, z) = N \sum_{i=1}^{N} |\phi_i(x, y, z)|^2 \tag{17}$$

This is simply the sum of the probabilities that the electron in orbital i is located at x, y, z. In general, we won't know the exact form of the orbitals. This is what we will be refining with our energy functional. Often researches tend to write a given orbital in the following form:

$$\phi_i(x, y, z) = \sum_{\mu=1}^{K} C_{\mu,i} \tilde{\phi_\mu}(x, y, z) \tag{18}$$

This is simply a linear combination of basis functions $\tilde{\phi_\mu}(x, y, z)$. This is essentially exactly the same as fitting arbitrary functions to some data, such as a neural network or a linear regression model. The key difference is that we wont be fitting data, rather we will be enforcing self-consistency [20] and minimization through the energy functional. The energy functional uses the density in the following way:[4]

$$E_{\text{Elec.}}[\rho] = T[\rho] + E_{eN}[\rho] + E_{ee}[\rho] \tag{19}$$

The terms of this functional are the electron kinetic energy, the electron-nuclei attraction, and the electron-electron repulsion. The easiest to compute is the electron-nuclei interaction. This will just be Coulomb's law integrated over the density:

$$E_{eN}[\rho] = -\sum_{A}^{\text{Nucl.}} \int \frac{Z_A \rho(\mathbf{r})}{|\mathbf{R}_A - \mathbf{r}|} d\mathbf{r} \tag{20}$$

[4]The constant nuclei energy is missing from this expression, it makes no change to the Eigenfunctions so we don't mind skipping it.

As stated previously, the kinetic energy is not known exactly. However, by constructing our density in terms of Hartree Fock theory we can use their form as a good estimate. This portion is defined as T_S.

$$T_S[\rho] = -\frac{1}{2}\sum_{i=1}^{N}\langle\phi_i(\mathbf{r})|\nabla^2|\phi_i(\mathbf{r})\rangle \tag{21}$$

Similarly, the potential as a known form. The Coulombic repulsion.

$$J[\rho] = \int\int \frac{\rho(\mathbf{r})\rho(\mathbf{r}')}{|\mathbf{r}-\mathbf{r}'|}d\mathbf{r}d\mathbf{r}' \tag{22}$$

This then gives the total energy functional as:

$$E_{\text{Elec.}}[\rho] = T_S[\rho] + E_{eN}[\rho] + J[\rho] + E_{xc}[\rho] \tag{23}$$

Where the last term is the exchange correlation functional. This is defined as the difference between what we dont know and what we do know:

$$E_{xc}[\rho] = (T[\rho] - T_S[\rho]) + (E_{ee}[\rho] - J[\rho]) \tag{24}$$

This is a correction term, where it contains any kinetic energy missed by the Hartree Fock picture as well as any extra potential energy contributions from exchange and correlation. Each piece of the energy functional is exactly computable except for the exchange correlation functional. Due to the exchange correlation functional being unknown, we require some different approximation schemes. This is the crux of any DFT calculation based in Kohn and Sham's scheme. Combining all of these terms into one equation, we get the following:

$$E_{\text{Elec.}}[\rho] = -\frac{1}{2}\sum_{i=1}^{N}\langle\phi_i(\mathbf{r})|\nabla^2|\phi_i(\mathbf{r})\rangle - \sum_{A}^{\text{Nucl.}}\int\frac{Z_A\rho(\mathbf{r})}{|\mathbf{R}_A-\mathbf{r}|}d\mathbf{r} + \int\int\frac{\rho(\mathbf{r})\rho(\mathbf{r}')}{|\mathbf{r}-\mathbf{r}'|}d\mathbf{r}d\mathbf{r}' + E_{xc}[\rho] \tag{25}$$

A specific exchange-correlation functional is the local density approximation (LDA). This is done by splitting the exchange and the correlation effects. Dirac and Slater formulated this exchange piece by modeling a uniform electron gas in their earlier works [22].

$$E_{xc}[\rho] = \int\rho(\mathbf{r})(E_x(\rho) + E_c(\rho)) \tag{26}$$

$$E_x(\rho) = -c_x\int\rho(\mathbf{r})^{\frac{4}{3}}d\mathbf{r} \tag{27}$$

Then the correlation term can be found via a Monte Carlo fitting procedure. With the entire functional established. How do we fully solve for the orbitals as well as the ground state energy to attain our potential energy surface? We can take a functional derivative of the energy functional and set it to zero.

$$\frac{\delta E_{\text{Elec.}}[\rho]}{\delta\rho} = 0 \tag{28}$$

However, this procedure does not enforce the orbitals to to be orthogonal. We can ensure that it will by creating a Lagrangian with the included Lagrange multiplier.

$$L[\rho] = E_{\text{Elec.}}[\rho] - \sum_{i=1}^{N}\epsilon_i\left(\int\phi_i(\mathbf{r})^*\phi_i(\mathbf{r})d\mathbf{r} - 1\right) \tag{29}$$

Interestingly enough it can be shown that minimizing this with respect to ρ is the same as minimizing with respect to each of the orbitals on their own. Taking the functional derivative of the Lagrangian with respect to $\phi_i^*(\mathbf{r})$ gives:

$$\left(-\frac{1}{2}\nabla^2 - \sum_A^{\text{Nucl.}} \frac{Z_A}{|\mathbf{R}_A - \mathbf{r}|} + \int \frac{\rho(\mathbf{r}')}{|\mathbf{r} - \mathbf{r}'|} d\mathbf{r}' \right) \phi_i(\mathbf{r}) + \frac{\delta E_{\text{xc}}[\rho]}{\delta \phi_i^*} = \epsilon_i \phi_i(\mathbf{r}) \tag{30}$$

Noting that the exchange correlation portion of the previous equation is a functional of the density and not the orbital. We can use to chain rule to show that this is just:

$$\frac{\delta E_{\text{xc}}[\rho]}{\delta \phi_i^*} = \int \frac{\delta E_{\text{xc}}[\rho]}{\delta \rho} \frac{\delta \rho}{\delta \phi_i} d\mathbf{r} = \frac{\delta E_{\text{xc}}[\rho]}{\delta \rho} \phi_i(\mathbf{r}) \tag{31}$$

What this now means is we can define a new pseudo-potential v_{xc}:

$$v_{xc}(\mathbf{r}) = \frac{\delta E_{\text{xc}}[\rho]}{\delta \rho} \tag{32}$$

For the local density approximation this becomes:

$$v_{xc}(\mathbf{r}) = -c_x \rho(\mathbf{r})^{\frac{1}{3}} + v_c(\mathbf{r}) \tag{33}$$

Finally we arrive at a new equation for the orbitals that is solvable.

$$\left(-\frac{1}{2}\nabla^2 - \sum_A^{\text{Nucl.}} \frac{Z_A}{|\mathbf{R}_A - \mathbf{r}|} + \int \frac{\rho(\mathbf{r}')}{|\mathbf{r} - \mathbf{r}'|} d\mathbf{r}' + v_{xc}(\mathbf{r}) \right) \phi_i(\mathbf{r}) = \epsilon_i \phi_i(\mathbf{r}) \tag{34}$$

This looks like N time independent Schrodinger equations for a set of non-interacting electron orbitals in an effective potential. The key point is that we can now solve a fictitious non-interacting system but we can attain the same ground state energy for an interacting one! Once we obtain the correct orbitals, to send that information upwards to the nuclei simply compute the energy from the original functional $E[\rho]$.

There are many more functional to consider. The LDA only considers the values of the functional at a given point in space. A clear extension would be to include the gradients within the expression. There are also the hybrid functionals which really jump started the methods popularity as a whole.

2.3 Potential Energy Surfaces and Geometry Optimization

The main application of DFT to catalysis is in geometry optimization [23] [24] [25] [26] [27] [28]. Given a geometry, it is possible to compute the energy due to electronic effects by solving the set of equations defined by equation 34. This then implies we can create a 3N dimensional surface, where the inputs are the atomic nucleus co-ordinates and the output is their corresponding electric structure ground state. This surface is defined by equation 10. There are multiple observable quantities that we can compute with this surface. However, in catalysis the primary use case is to perform geometry optimization and discover possible reaction pathways [29] [30].

A potential energy surface (PES) need not have curvature as we have defined it. As an example we can consider one molecule where we apply only a translation and a rotation, not changing the relative distances between atoms. This type of motion along the PES would cause no change in energy, therefore we can remove this type of motion from the PES and rewrite it in terms of only the types of motions that effect the energy. However, we can cause a change in energy by changing the distance between two atoms that we believe are bonded. In 2017 Tamukong et. al. published a study using DFT-in-DFT embedding theory as well as the presented Kohn Sham DFT to compute the energy as a function of bond length in multiple materials [25]. Relative energy of the dissociation of LiF is presented in figure 1

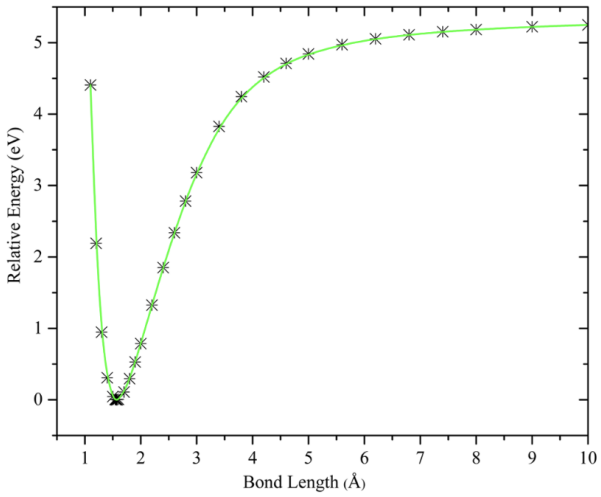

Figure 1: *Relative energy dissociation curves of LiF obtained with the embedding-with-external-orbital-orthogonality DFT-in-DFT (green) and KS-DFT calculations (black). The green curve completely obscures the KS-DFT curve* - Tamukong et. al.

Rather than just breaking a bond, we can cause more complex changes in our geometry. Within catalysis, mapping out the structure/energy of the reactants and the products as a reaction proceeds is of primary importance. In 1999 Niu and Hall from Texas A&M discussed the nuances of this process in a review on the applications to transition metal complexes in catalysis [8]. A key step in this procedure is the identification of equilibrium state minima, transition state saddle points, as well as high order energy maxima saddle points. Chemical reactions tends to follow paths between these points. Of course a reaction proceeds statistically, following a stochastic process type structure. However, we can model the most statistically significant path by considering those with the smallest free energy barriers. We can define each of these points mathematically. Consider the input/output relationship between the PES and the nuclear co-ordinates.

$$E_{\text{Elec.}} : \mathbb{R}^{\#\text{ of Nucl.}} \mapsto \mathbb{R} \tag{35}$$

This is a vector equation. This means if we differentiate the energy with respect to each atomic co-ordinate we get a vector. When the derivative of this vector is zero, that implies we are at a stationary point.

$$\frac{dE_{\text{Elec.}}}{d\mathbf{R}} : \mathbb{R}^{\#\text{ of Nucl.}} \mapsto \mathbb{R}^{\#\text{ of Nucl.}} \tag{36}$$

$$\left(\frac{dE_{\text{Elec.}}(\mathbf{R})}{d\mathbf{R}}\right) = \mathbf{0} \implies \mathbf{R} = \text{Stationary Point} \tag{37}$$

Every stationary point can be further classified by computing the second derivative, the Hessian matrix $\mathbf{H}$.

$$\mathbf{H} : \mathbb{R}^{\#\text{ of Nucl.}} \mapsto \mathbb{R}^{\#\text{ of Nucl.}} \times \mathbb{R}^{\#\text{ of Nucl.}} \tag{38}$$

If $\mathbf{H}$ has all positive eigenvalues, the point in question is a minima/equilibrium geometry. These minima correspond to initial stable reactant states, or final stable product states. The magnitude determines exactly how stable the minima is. Note as well, this implies they are a minima in every dimension. If $\mathbf{H}$ has one negative eigenvalue, then the state $\mathbf{R}$ is a transition state between reactants and products. These are called transition states because because they must be crossed as a set of nuclei move from products to reactants. These states are minima in every dimension except one. If there is a multiple negative eigenvalues, this is called a high order saddle point and are generally of minimal chemical significance. These are minima in every dimension, aside from those corresponding to negative eigenvalues. One can consider a path between these points as the reaction co-ordinate. A cartoonish presentation of a PES with one transition state and two equilibrium geometries can be seen in figure 2.

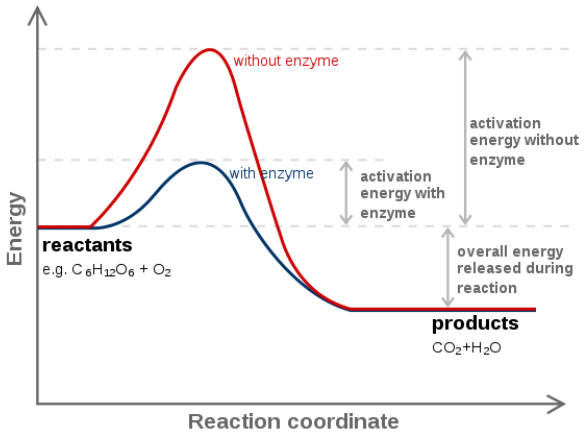

Figure 2: Cartoonish representation of an exothermic chemical reaction. The red curve is an uncatalyzed chemical reaction, the blue is catalyzed by an enzyme. Figure taken from the reaction co-ordinate Wikipedia page.

Alongside the eigenvalues of the Hessian matrix, these can communicate a tons of information about which components are important in a reaction. By scaling the eigenvectors and animating how the geometry changes, one can visualize exactly which atoms are important for a reaction. This allows us to quantify which steps a catalyst is contributing to, or if it contributing at all. This all depends on finding these transition states. Searching for transition states is generally more difficult than searching for equilibrium geometries. Researchers resolve this by choosing informed starting geometries as well as tailored algorithms such as graph-based methods [31], permutationally invariant reaction discovery [32], as well as numerous automatic data driven methods [33].

3 DFT In Catalysis

Although the primary use case of DFT is geometry optimization and reaction pathways, there are many possible alternative use cases. It would be near impossible to go through every specific method employed. Therefore, this section aims to outline a few specific examples to give a feel for the breadth of the DFT methodology in catalyst development.

3.1 A Study on the Coking of Ni Catalysts

As a illustrative example, in 2002 Bengaard and coworkers used geometry optimization to quantify the difference between Ni(211) step and Ni(111) sites in the steam reforming reaction.

$$CH_4 + H_2O \rightleftharpoons CO + 3H_2 \tag{39}$$

They did so using the generalize gradient approximation (GGA) energy functional. The GGA functional builds upon the presented LDA functional by including derivative information. To model the Ni surface, Bengaard used a periodic repeating supercell. Using a fully periodic slab can make the calculations of the energy easier in comparison to having it be only periodic in 2 dimensions. Note that the slabs must be sufficiently far from each other that the electron density goes to zero between the slabs. By taking possible components in the reaction and optimizing their geometry in the presence of the different Ni sites they arrived a set of energies for each step in the reaction. Their results are presented in figure 3.

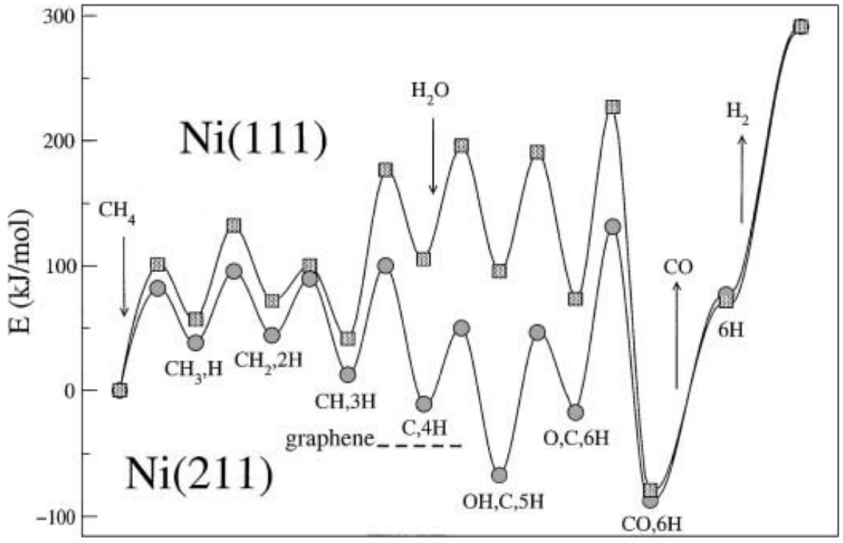

Figure 3: *Energies for the species on Ni(211) and Ni(111). All energies are relative to CH4 and H2O in the gas phase and calculated using the results for the individual species.* - Bengaard

Their results convey two main messages. The Ni(211) steps are more reactive than the Ni(111) surface sites. Notably the rate determining step, activating methane. Similarly, the atomic carbon is much more stable on step sites than surface sites. This implies that the coking process is more likely to nucleate on step sites. This hints at a potential method to increase the recyclability of the catalyst. If you can strategically engineer the step sites, then the nucleation is more unlikely to occur.

Relative Energies (kJ/mol) per Carbon Atom on the Two Surfaces, and the Edge Energy for Graphene on Ni(111)

	Ni(211) atomic C		Ni(111)		
	1C:2Ni edge atoms	1C:1Ni edge atom	Atomic C	Monolayer graphene	Graphene edge energy
E (kJ/mol)	0	43	97	−33	172

Figure 4: A table of energies to decipher coking on Ni catalysts.

A specific consideration they looked into was the formation of graphene monolayers, and graphite islands. Through DFT they showed the graphene layers are even more stable than the individual atomic carbon adsorbed to the step site. This explains the carbon whisker and coking observed in actual industrial processes. It happens because it is vastly more energetically favorable than proceeding through the reaction. This process is likely to nucleate on the step sites due to the lower energies computed there. However, they also found that as the step sites get covered by carbon, the resulting energy increases. This implies that the initial; formation of the layer is unfavorable, but once a critical mass of carbons is reached it becomes a graphene monolayer which is vastly more stable. This means, if we can prevent that critical mass from forming then the bulk of the coking process can be prevented. In order to estimate the critical mass, energy computations of the free carbon, step bound carbon, carbon edge, and graphene monolayer must be calculated. Bengaard's calculations are presented in table 4. Using these they estimated the critical mass of carbons as ~ 80 atoms. This corresponds to a step size of ~ 25 angstroms. This gives a goal for instrumentalists, if they are able to engineer the facets of their catalyst to be smaller than ~ 25 angstroms then graphite is less likely to form. Experimental observations of weight of carbon versus process time do in fact show an initiation period with an increasing rate of carbon formation before the coking rate stagnates [34] [35]. Bengaard claims that this could be due to the initial unfavorability of the coking process.

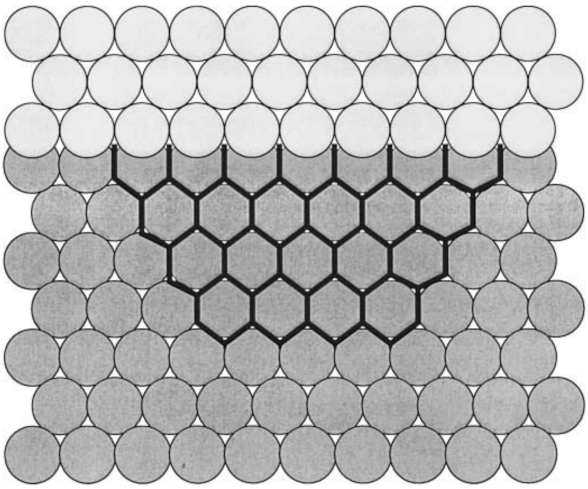

Figure 5: *The graphene island used in the model is semihexagonal and attached to a step edge. - Bengaard*

3.2 Discovering Novel Ammonia Synthesis Reaction Pathways with DFT

In 2005 Honkala and coworkers performed an ab-initio study on ammonia synthesis [26]. They do so utilizing density functional theory. They then developed a more accurate kinetic model that includes the catalytic reaction over a packed bed of a high surface area nanoparticle catalyst that takes into account the DFT computations they performed. Specifically they considered a ruthenium catalyst with support and compared it with high agreement to industrially relevant processes while only considering the particle size distribution as an experimental input. To reiterate, they used the size distribution to create a specific DFT geometry distribution which can then be used to estimate pathways and rates.The initial part of the characterization process was to model the potential energy surface as a function of the molecular geometry. This showed the expected result that the step sites are much more reactive than the terrace sites. This also resulted in a reaction pathway. The resulting pathway can be seen in in figure 6.

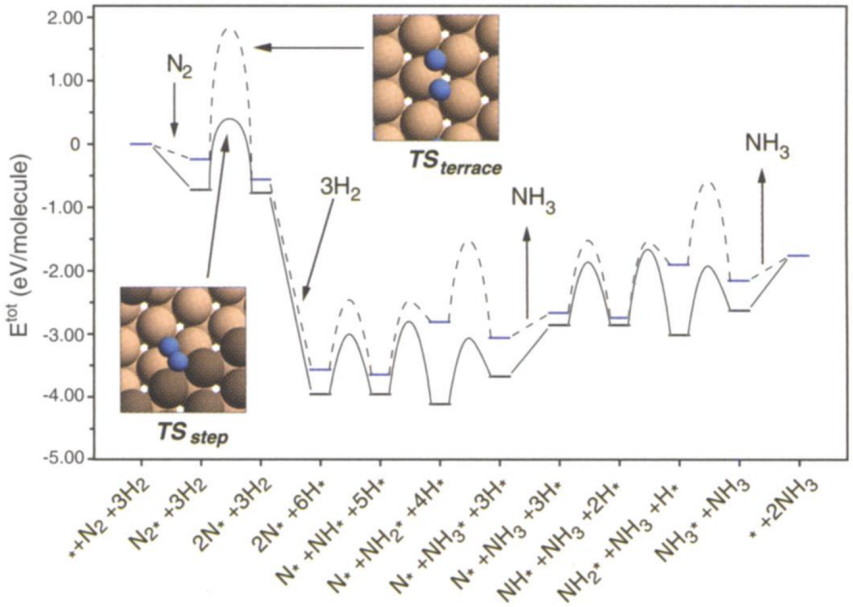

Figure 6: *The calculated potential energy diagram for NH3 synthesis from N2 and H2 over close-packed (001) and stepped Ru surfaces (20). A * denotes an empty site and X* an adsorbed species. The configuration of the transition states (TS) for N_2 dissociation over the terrace and step sites is shown in the insets.* - Honkala

Combining their energies with a harmonic transition state theory they were able to show that the N2 dissociation is the rate limiting step (RDS) under realistic operating conditions. Then they calculated the rate constant for the RDS with the Arrhenius form based on the energy computed with the DFT energy surface. This means that the rate would change as a function of the energy for a specific nuclei geometry. Taking these results they used a similar method to the generic heterogeneous site coverage analysis to attain an overall rate law in terms of partial pressures. However they modified the probability of the N2 adsorption. To do so they utilized a grand canonical Monte Carlo simulation.

They analyzed roughly 1000 different particles using TEM to attain a size distribution. Rather than direct counting they calculated the surface energy to attain the fraction of sites as a function of particle size and then used the Wulff construction to estimate particle shape [36]. They specifically neglected the support and commented that their analysis on this step was very crude, however they were still in good agreement with the experimental results. There is most likely uncertainty in their estimated completeness of the Wulff polyhedra. They believe that there may be more partly filled layers, but their estimate seems like a lower bound. They then showed that the rate was 3 to 20 times smaller than the experimental rate. However, considering the lack of empirical input their results were promising. They comment on the lack of exact agreement by noting that an misprediction of 0.25 eV of energy can cause a 148 factor difference in the rate of an elementary reaction step at 600 K. To study this effect they then mixed two different energy surfaces derived from different functions in their DFT calculations to estimate the rate and showed that the overall rate was insensitive to the choice of functional mixing. This implies that misprediction of the energy for a specific elementary may not be controlling their faulty predictions. Rather, it is controlled by the faulty estimation of the number of active sites or a faulty description of bonded interactions in their monte carlo simulations. By decreasing the stability of adsorbed H relative to the NHX species by 0.06 eV they were able to attain a match to experiments at all temperatures and flows, showing that initial faulty predictions were not due to their DFT calculations. Overall, this outlines a procedure for attaining mechanistic understanding of catalysis using DFT and presents a promising future for the field.

3.3 Molecular Dynamics: ReaxFF

A clear use case is the propagation of the potential energy surface into molecular dynamics simulations. Molecular dynamics (MD) is one of the most adopted methods in physical chemistry. However MD has some key issues that can prevent it's ability to match experimental data due to faulty PES inputs. The most common form of MD is driven by two body potential energy surfaces. These two body energy surfaces are also commonly fit to one experimental observable with a lack of care for all others. This causes an overfitting trend in most MD simulations. To resolve this, there have been multiple key developments. Rather than going through them all, the ReaxFF [11][12] bond order force field developed by Goddard is only presented for brevity. Both of these methods are empirically fit to DFT calculations rather than experimental datum. Due to DFT's high accuracy when compared to most experimental observations, the expectation is that an approximate DFT calculation through ReaxFF potentials will be just as accurate. This section aims to outline the basics of these methods so researchers can apply them to their catalytic systems. Then a specific calculation will be presented dealing with homogeneous catalysis using ReaxFF.

ReaxFF acts similarly to a two body potential energy surface by taking into account the pairwise distance between nuclei to compute the energy. This opposes the paradigm of DFT, in DFT they take into account not only the distances but the absolute position of every atom. This informs the calculation about three body angular and n-body effects. To achieve a similar ideal, ReaxFF also extends upon the pairwise distance calculations by including bond order as a direct input. With the inputs to the force field established, ReaxFF simply chooses a functional form and empirically fits multiple constants within it to reproduce DFT data. An example geometry optimization for ethan using both energetic methods is presented in figure 7.

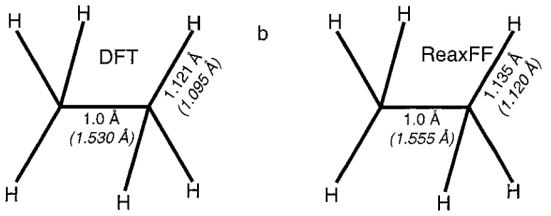

Figure 7: *Effects of shortening of the C-C bond length in ethane to 1.0 Å on the relaxed C-H bond lengths as calculated by DFT and ReaxFF. Equilibrium C-C and C-H bond lengths are in italics and brackets.* - C. T. van Duin

Researchers can then compute newtons equations of motion on the PES to resolve the dynamics of the classical nuclei. In principle, this can be done by DFT. However, it is much to slow to do this type of calculation on systems larger than

20 atoms. By then observing the time required for the system to fully react, we can obtain reaction rates for a catalyst. Similarly, by using theories from statistical mechanics researchers can estimate any thermodynamic observable for a catalyst system.

Researchers Feng, Jiang, and Luo, from University College London performed a molecular dynamics study on platinum-decorated functionalized graphene sheet catalyzed methane oxidation using the ReaxFF force field [37]. They built four different periodic systems with different sizes but the same density. Their base system contained 50 CH4 and 100 O2 molecules. They then duplicated it with three different catalysts, a Functionalized Graphene Sheet, two Tetrahedral Pt Clusters and a Pt-decorated Functionalized Graphene Sheet. They adopted a canonical NVT ensemble with a Nose-Hoover thermostat. To get the initial configuration into an energetically favorable state they performed a conjugate gradient algorithm. An initial equilibration procedure was done for 100 ps with a 0.1 fs timestep. Similarly to previous research [38] they turned off the C–O and H–O bond interactions in the force field to prevent reactions during equilibration. They disabled reactions with the catalysts during equilibration as well. Equilibration of the functionalized graphene sheets were performed separately to maintain their crystal structure. Once these steps were done, they ran a data collection period for 4000 ps for ramped temperature simulations and 1000 ps for constant temperature. They noted that performing the reaction at a higher temperature can aid in the computational slowdown caused by the smaller atomic motion at low temperatures. A 0.2 bond order cutoff is used for analysis of species formation. This allows for more sensitivity to different reaction pathways. Overall they averaged over three runs of each simulation type for their results. Each initial configuration had unique geometries so as to not get statistically dependent results. The ramping occurred from 300 to 3000 kelvin at 0.9 K per ps. The constant temperature ran at 3000 kelvin. The fastest reaction rate was observed for the platinum-decorated functionalized graphene sheet. Whereas the functionalized graphene sheet was slightly faster for the first 3000 ps of the ramped simulation but the platinum alone sped up significantly afterwards. Overall, from best to worst they ranked: platinum-decorated functionalized graphene sheet, platinum on its own, graphene sheet, no catalyst.They then presented a graphical reaction pathway obtained from their simulations. The platinum-decorated functionalized graphene sheet combination increased catalytic activity by lowering the activation energy by 73%. In their reaction mechanisms, the edge of the graphene sheet seemed to oxidize more at the edge. Their pathways indicated the methane oxidation with their catalyst is initiated by cleaving the C–H bond for the production of hydroxyl. Most importantly, the most active sites get consumed quickly and the platinum-decorated functionalized graphene sheet quickly reduces to the graphene sheet. This research shows that the ReaxFF DFT method can be used to engineer good catalysts and should be heavily utilized in characterization schemes.

4 Conclusions

This paper has highlighted the vital role that density functional theory plays in advancing our understanding of catalytic processes. By employing DFT, researchers gain the ability to explore potential energy surfaces, pinpoint energy minima and saddle points, and unravel the intricate pathways that chemical reactions traverse. The exploration of the fundamentals of electronic structure theory, the Born-Oppenheimer approximation, the Hohenberg-Kohn theorems, and the Kohn-Sham methodology has laid the groundwork for new research exploiting the intricacies of DFT. The three illustrative calculations—scrutinizing coking on Ni surfaces, investigating ammonia synthesis reaction pathways, and employing the ReaxFF force field for thermodynamic assessments—underscore the versatility of DFT in addressing a spectrum of challenges in catalysis research. By bridging the theoretical and applied domains, DFT not only amplifies our capacity to interpret experimental data but also steers the design of innovative catalysts that will lay the groundwork for more efficient, effective, and recyclable catalysts.

Acknowledgments

This was was supported in part by the teaching of Professor M. Nigra of the University of Utah Chemical Engineering Department.

References

(1) Guerrero-Pérez, M. O.; Patience, G. S. *The Canadian Journal of Chemical Engineering* **2020**, *98*, _eprint: https://onlinelibrary.wiley.com/doi/pdf/10.1002/cjce.23664, 25–33.

(2) Bazin, D.; Guczi, L.; Lynch, J. *Applied Catalysis A: General* **2002**, *226*, 87–113.

(3) Yang, J. C.; Small, M. W.; Grieshaber, R. V.; Nuzzo, R. G. *Chemical Society Reviews* **2012**, *41*, Publisher: The Royal Society of Chemistry, 8179–8194.

(4) Misic, M.; Đurđević, Đ.; Tomasevic, M. In 2012, pp 289–294.

(5) McArdle, S.; Endo, S.; Aspuru-Guzik, A.; Benjamin, S. C.; Yuan, X. *Rev. Mod. Phys.* **2020**, *92*, 015003.

(6) Nørskov, J. K.; Abild-Pedersen, F.; Studt, F.; Bligaard, T. *Proceedings of the National Academy of Sciences* **2011**, *108*, Publisher: Proceedings of the National Academy of Sciences, 937–943.

(7) Mircescu, N. E.; Oltean, M.; Chiş, V.; Leopold, N. *Vibrational Spectroscopy* **2012**, *62*, 165–171.

(8) Niu, S.; Hall, M. B. *Chemical Reviews* **2000**, *100*, Publisher: American Chemical Society, 353–406.

(9) Altaf, A. A.; Kausar, S.; Badshah, A. In *Density Functional Calculations*, Yang, G., Ed.; IntechOpen: Rijeka, 2018; Chapter 5.

(10) Frisch, M. J. et al. Gaussian~16 Revision C.01, Gaussian Inc. Wallingford CT, 2016.

(11) Van Duin, A. C. T.; Dasgupta, S.; Lorant, F.; Goddard, W. A. *The Journal of Physical Chemistry A* **2001**, *105*, Publisher: American Chemical Society, 9396–9409.

(12) Senftle, T. P.; Hong, S.; Islam, M. M.; Kylasa, S. B.; Zheng, Y.; Shin, Y. K.; Junkermeier, C.; Engel-Herbert, R.; Janik, M. J.; Aktulga, H. M.; Verstraelen, T.; Grama, A.; van Duin, A. C. T. *npj Computational Materials* **2016**, *2*, 15011.

(13) Born, M.; Oppenheimer, R. *Annalen der Physik* **1927**, *389*, _eprint: https://onlinelibrary.wiley.com/doi/pdf/10.1002/andp.19273892002, 457–484.

(14) Valeev, E. F.; Sherrill, C. D. *The Journal of Chemical Physics* **2003**, *118*, 3921–3927.

(15) Fock, V. *Zeitschrift für Physik* **1930**, *61*, 126–148.

(16) Hückel, E. *Zeitschrift für Physik* **1931**, *70*, 204–286.

(17) Shao, Y. et al. *Molecular Physics* **2015**, *113*, Publisher: Taylor & Francis _eprint: https://doi.org/10.1080/00268976.2014.952696, 184–215.

(18) Hohenberg, P.; Kohn, W. *Physical Review* **1964**, *136*, Publisher: American Physical Society, B864–B871.

(19) Pauli, W. In *Writings on Physics and Philosophy*, Enz, C. P., Von Meyenn, K., Eds.; Springer Berlin Heidelberg: Berlin, Heidelberg, 1994, pp 165–181.

(20) Kohn, W.; Sham, L. J. *Physical Review* **1965**, *140*, Publisher: American Physical Society, A1133–A1138.

(21) Slater, J. C. *Physical Review* **1929**, *34*, Publisher: American Physical Society, 1293–1322.

(22) Dirac, P. a. M. *Mathematical Proceedings of the Cambridge Philosophical Society* **1930**, *26*, Publisher: Cambridge University Press, 376–385.

(23) Bleakley, K.; Hu, P. *Journal of the American Chemical Society* **1999**, *121*, 7644–7652.

(24) Braga, A. A. C.; Ujaque, G.; Maseras, F. *Organometallics* **2006**, *25*, Publisher: American Chemical Society, 3647–3658.

(25) Tamukong, P. K.; Khait, Y. G.; Hoffmann, M. R. *The Journal of Physical Chemistry A* **2017**, *121*, Publisher: American Chemical Society, 256–264.

(26) Honkala, K.; Hellman, A.; Remediakis, I. N.; Logadottir, A.; Carlsson, A.; Dahl, S.; Christensen, C. H.; Nørskov, J. K. *Science (New York, N.Y.)* **2005**, *307*, 555–558.

(27) Borowiecki, T. *Applied Catalysis* **1982**, *4*, 223–231.

(28) Bengaard, H. S.; Nørskov, J. K.; Sehested, J.; Clausen, B. S.; Nielsen, L. P.; Molenbroek, A. M.; Rostrup-Nielsen, J. R. *Journal of Catalysis* **2002**, *209*, 365–384.

(29) Koga, N.; Daniel, C.; Han, J.; Fu, X. Y.; Morokuma, K. *Journal of the American Chemical Society* **1987**, *109*, Publisher: American Chemical Society, 3455–3456.

(30) Farberow, C. A.; Dumesic, J. A.; Mavrikakis, M. *ACS Catalysis* **2014**, *4*, Publisher: American Chemical Society, 3307–3319.

(31) Ismail, I.; Chantreau Majerus, R.; Habershon, S. *The Journal of Physical Chemistry A* **2022**, *126*, Publisher: American Chemical Society, 7051–7069.

(32) Robertson, C.; Hyland, R.; Lacey, A. J. D.; Havens, S.; Habershon, S. *Journal of Chemical Theory and Computation* **2021**, *17*, Publisher: American Chemical Society, 2307–2322.

(33) Puliyanda, A.; Srinivasan, K.; Sivaramakrishnan, K.; Prasad, V. *Digital Chemical Engineering* **2022**, *2*, 100009.

(34) Rostrup-Nielsen, J. R. In *Catalysis: Science and Technology Volume 5*, Anderson, J. R., Boudart, M., Eds.; Catalysis; Springer: Berlin, Heidelberg, 1984, pp 1–117.

(35) Alstrup, I.; Tavares, M.; Bernardo, C.; Sørensen, O.; Rostrup-Nielsen, J. *Materials and Corrosion* **1998**, *49*, 367–372.

(36) Wulff, G. *Zeitschrift für Kristallographie - Crystalline Materials* **1901**, *34*, 449–530.

(37) Feng, M.; Jiang, X. Z.; Luo, K. H. *Proceedings of the Combustion Institute* **2019**, *37*, 5473–5480.

(38) Page, A. J.; Moghtaderi, B. *The Journal of Physical Chemistry A* **2009**, *113*, Publisher: American Chemical Society, 1539–1547.